Contents lists available at ScienceDirect

Transactions of Nonferrous Metals Society of China

36(2026) 780−795

www.tnmsc.cn

Microstructural evolution and mechanical properties of titanium/steel composite plate during pure titaniumization in welding area

Hong-ting CHEN [a,b,c], Xue-feng LIU [a,b,c,*], Zhi-yan YANG [a,b,c], Xiao-liang LU [a]

[a] Beijing Advanced Innovation Center for Materials Genome Engineering, University of Science and Technology Beijing, Beijing 100083, China;

[b] Beijing Laboratory of Metallic Materials and Processing for Modern Transportation, University of Science and Technology Beijing, Beijing 100083, China;

[c] Key Laboratory for Advanced Materials Processing of Ministry of Education, University of Science and Technology Beijing, Beijing 100083, China

Abstract: The transformation of the dissimilar metals in the welding area into a single metal is an important method for achieving high-quality welded connection in the dissimilar metal laminated composite plate. In this study, a high-performance titanium/steel composite plate (TSCP) with pure titaniumization in the welding area was prepared by cold spraying, hot rolling and heat treatment processes. The results indicate that cold spraying achieves effective pre-composite deposition of titanium particles while inhibiting interfacial oxidation and Fe−Ti alloying reactions, producing a relatively dense pure titanium coating with a low porosity of only 1.2%. Hot rolling eliminates internal defects and promotes strong metallurgical bonding of the composite interface. The heat treatment promotes the recrystallization and reduces the dislocation density within the coating. The interfacial bonding strength of the welding area with pure titaniumization of TSCP is 257 MPa, and the tensile strength of that is 414 MPa, reaching 95.6% of the TSCP's base material.

Keywords: titanium/steel composite plate; cold spraying; welded transition joint; microstructure; mechanical properties

1 Introduction

The metal laminated composite plate (MLCP) is composed of two or more layered metals and inherits the excellent properties of the component layer metals. It is widely used in aerospace, rail transportation, petrochemicals, telecommunication, defense industries, and other fields [1−3]. Welding connection is a critical processing step in the application of MLCP. However, the physical and chemical properties of each component metal of MLCP are quite different. During the high-temperature welding and the process of metallurgical bonding, the MLCP is prone to alloying reactions at the composite interface and welded joints, forming hard and brittle intermetallic compounds (IMCs) [4−8]. This will seriously degrade the comprehensive performance of the composite interface and welded joints, affecting their service safety.

In view of the difficulty in achieving high-quality welded connection between dissimilar metals, dissimilar metal transition joints have been extensively researched and applied [9−13]. ZHANG et al [11] utilized a titanium/steel transition joint to weld titanium and steel, effectively transforming the welding of dissimilar metals into the welding of the single metal on both sides. This approach avoids the alloying reactions between dissimilar metals, thereby achieving high-quality welding formation.

Corresponding author: *Xue-feng LIU, Tel: +86-10-62333627, E-mail: liuxuefengbj@163.com

https://doi.org/10.1016/S1003-6326(25)66997-4

Received 6 June 2024; accepted 24 March 2025

Unlike the welding of dissimilar metals, MLCP is composed of dissimilar metals, and it is normally necessary to add cladding cover joints to achieve separate welding of dissimilar metals. However, this process may result in gaps or incomplete penetration defects in the welded joints, which are detrimental to service safety [14]. Therefore, considering the unique characteristics of MLCP, transforming the welding area into a single metal welding transition joint is an important method to solve the problem of welding formation.

Cold spraying is a solid-state deposition composite technology, which can deposit metal particles on a substrate with complex surface topographies [15]. The gas temperature used is far below the melting point of the raw material, effectively reducing the oxidation of the raw material and the alloying reaction of the dissimilar metals [16]. Currently, cold spraying technology has successfully achieved the preparation of coatings for copper, steel, titanium, aluminum and their alloys [17−20]. For example, ZHAO et al [20] prepared titanium/steel composite plate by depositing a titanium layer onto a steel matrix using cold spraying, and REN et al [17] prepared magnesium/aluminum composite plate by depositing an aluminum alloy layer onto a magnesium alloy matrix using cold spraying. Therefore, the cold spraying technique is expected to prepare single metal welded transition joints by depositing composite in the welding area of MLCP. However, the bonding between cold sprayed coating and substrate is often weak in nature [20,21], which is mainly connected by mechanical interlocking and localized metallurgical bonding [19,22,23]. Moreover, the cold spraying technology is primarily used for deposition on the surface of the single metal, and simultaneous deposition on the surface of two different metals has not been reported. In addition, cold-sprayed coatings usually contain pores and defects, which may adversely affect the mechanical properties of MLCP [24,25]. In contrast, hot rolling and heat treatment can be used to change the microstructure of the coating and composite interface, effectively eliminating defects and improving the mechanical properties of the coating and the composite interface [20,26,27].

In this study, the titanium/steel composite plate is selected as the research subject. By constructing a trapezoidal side composite interface structure in the welding area of the titanium/steel composite plate, the titanium/steel dissimilar metals in the welding area are transformed into the single pure titanium metal through cold spraying, hot rolling and heat treatment processes, thereby preparing a single pure titanium welded transition joint on the titanium/steel composite plate. The process of transforming titanium/steel dissimilar metals into the single pure titanium metal is simplified as the pure titaniumization. This study analyzed the microstructural evolution and mechanical properties near the composite interface in the pure titaniumization area and revealed their relationship. Therefore, this study provides a new idea for transforming the welding area into the single metal in MLCP, which will be helpful for solving the welding challenges of MLCP and advancing its application.

2 Experimental

2.1 Raw materials

The raw materials used were commercial TA2 titanium plate and Q235 steel plate with thicknesses of 2 and 4 mm, respectively. Titanium/steel composite plates with a thickness of 3 mm were prepared by single-pass cold rolling with 50% rolling reduction, and the detailed preparation process was described in Ref. [28]. The titanium/steel composite plate was cut into experimental samples with a size of 150 mm × 60 mm by wire cutting. The interface morphology of cold-rolled titanium/steel composite plate is shown in Fig. 1. The composite interface is tightly bonded without holes and other defects. The TA2 titanium powder particles with a purity of 99.9% were prepared by plasma rotating electrode method and supplied by Shanghai ST-Nano Science and Technology Co., Ltd.

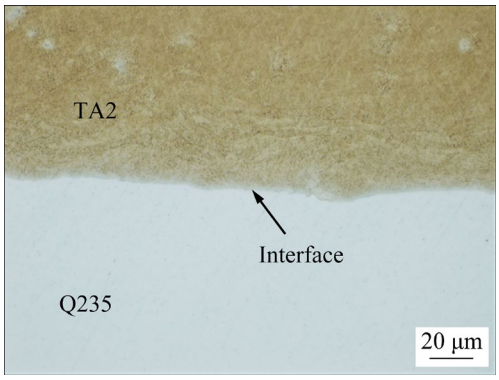

Fig. 1 Interface morphology of titanium/steel composite plate with cold-rolled bonding

2.2 Pure titaniumization in welding area

Figure 2 shows a schematic diagram of the process flow of pure titaniumization in the welding area of the titanium/steel composite plate, which mainly contains several steps of structural processing, surface treatment, cold spraying, heating, hot rolling and heat treatment. The titanium/steel composite plate with pure titaniumization in the welding area in the three states of cold spraying, hot rolling and heat treatment are marked as As-CS, As-SR and As-SRT, respectively. The details of each step are provided below.

Figure 2(a) shows the structural processing of the trapezoidal composite interface. The Q235 steel layer was completely removed from the welding area (diagonal line), and the TA2 titanium cladding was retained (red area). The width of the processed area for pure titaniumization was 25 mm, and the cold spraying angle (the angle between the spraying gun and the base surface) was 60°.

Before cold spraying, the composite surface underwent mechanically polishing and sandblasting to remove oxides and contaminants, exposing fresh metal, as shown in Fig. 2(b). The model of cold spraying equipment was Impact 5/11. Nitrogen (N_2) was used as the propellant gas in the cold spraying process, and the gas temperature and pressure were set as 760 °C and 4.7 MPa, respectively. The distance between the nozzle outlet and the upper surface of the titanium/steel composite plate was maintained at 25 mm. The nozzle moving speed was 50 mm/s and the running track spacing was 2 mm. The titanium coating (S-Ti) with the desired thickness was prepared by spraying in two passes to obtain the As-CS sample, as shown in Fig. 2(c). After spraying, the surface of the coating was polished and smoothed in preparation for subsequent hot rolling process.

The As-CS sample was heated at 850 °C for 20 min (Fig. 2(d)), and then immediately processed by hot rolling (Fig. 2(e)). The total rolling reduction rate was approximately 33%, resulting in the preparation of As-SR sample with a thickness of 2 mm. In order to observe the effect of the heating stage on the microstructure of the composite interface, the As-CS sample was heated at 850 °C for 20 min and subsequently air-cooled. The sample in the heated state was labeled as As-SH. The As-SR sample was heated at 900 °C for 10 min (Fig. 2(f)), followed by air-cooling to obtain the As-SRT sample.

2.3 Microstructure characterization and properties testing

The micromorphologies of As-CS, As-SH, As-SR and As-SRT samples were all taken from the surface of TD−ND plane. The low magnification macroscopic morphology was characterized by the optical microscope (Olympus BX53). The etching reagents used for titanium and steel were a modified Kroll reagent (60 mL H_2O+3.5 mL HF+1 mL HNO_3+

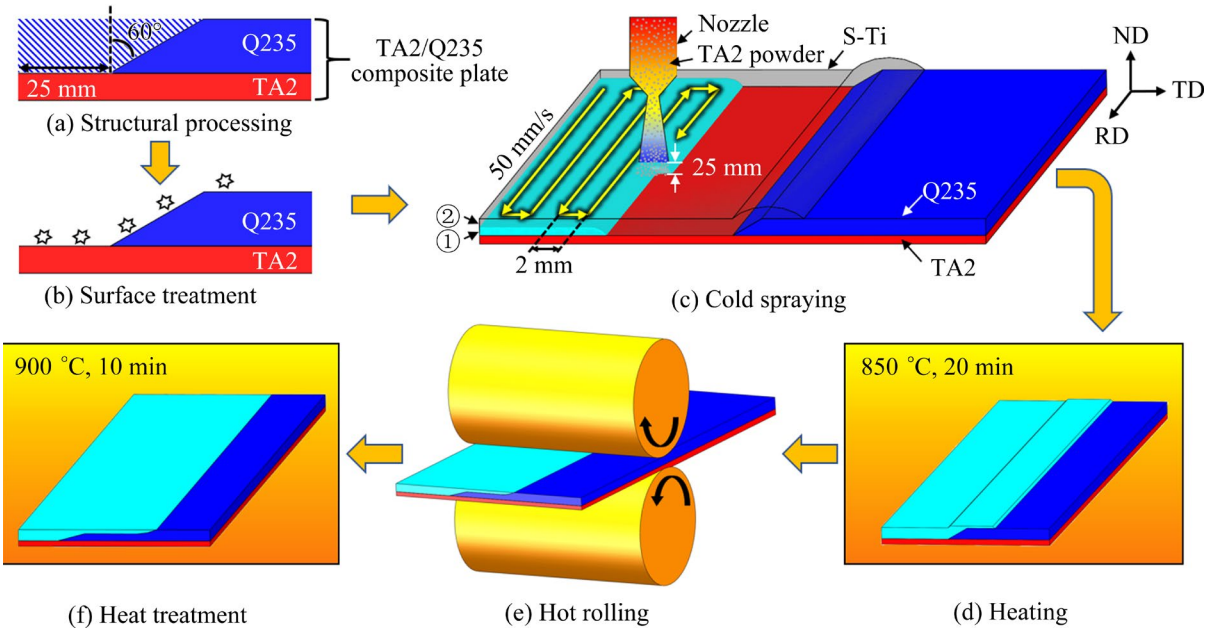

Fig. 2 Schematic diagram of process flow for pure titaniumization in welding area of titanium/steel composite plate

1 g MgF) and a 4 wt.% nitrate−alcohol, respectively. The microstructure morphology of the samples was characterized and analyzed by the field emission scanning electron microscope (SEM, Gemini SEM 500) with an energy dispersive spectrometer (EDS, Ultim Max 40). The porosity in the coating of As-CS sample was analyzed by ImageJ software, and the statistical area was about 0.48 mm^2. Samples for electron backscattering diffraction (EBSD) measurements were prepared by argon ion polishing method. The recrystallization and dislocation density distribution of the S-Ti/Q235 composite interface were tested and analyzed by EBSD and HKL Channel 5 software. The scanning step of EBSD was 0.6 μm. TEM samples were prepared by the focused ion beam (Helios Nanolab 600i-FIB), and the microscopic morphology and elemental distribution of the samples were characterized by transmission electron microscope (TEM, FEI Titan G2). The physical phases of the peeling composite interface were analyzed by X-ray diffractometer (XRD, SmartLab) within a scanning range of 30°−80°.

The mechanical properties were tested with a WDW−10E universal materials testing machine. The dimensions and the sampling location of the tensile and shear test specimens are shown in Fig. 3. The tensile rate is 1×10^{-3} s^{-1}, and the shear rate is 1 mm/min. Three samples were tested in each group, and the average of the three samples was taken as the mechanical properties.

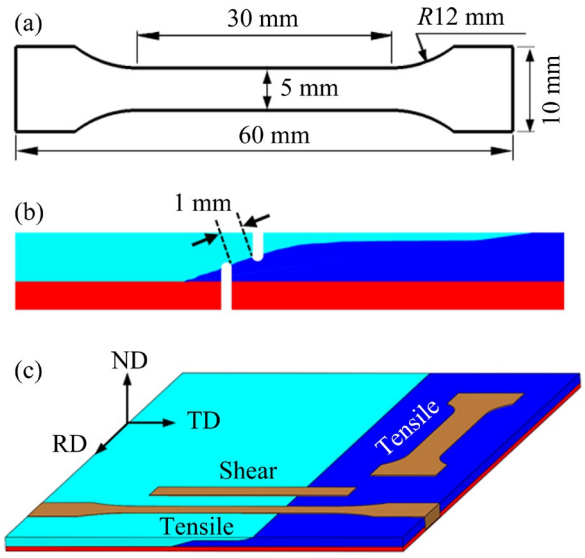

Fig. 3 Schematic diagrams of dimensions for tensile (a) and shear (b) test specimens, and sampling location (c)

3 Results

3.1 TA2 powder characteristics

The morphology, particle size distribution and XRD pattern of TA2 powder are shown in Fig. 4. It can be observed from the figure that the TA2 powder is a spherical particle (Fig. 4(a)). The particle size distribution of TA2 powder was measured by laser diffraction particle size analyzer, which ranged from 4 to 30 μm with a median diameter of 12.0 μm (Fig. 4(b)). The XRD analysis reveals that the phase structure of TA2 powder is α-Ti, without obvious impurities and oxidation (Fig. 4(c)).

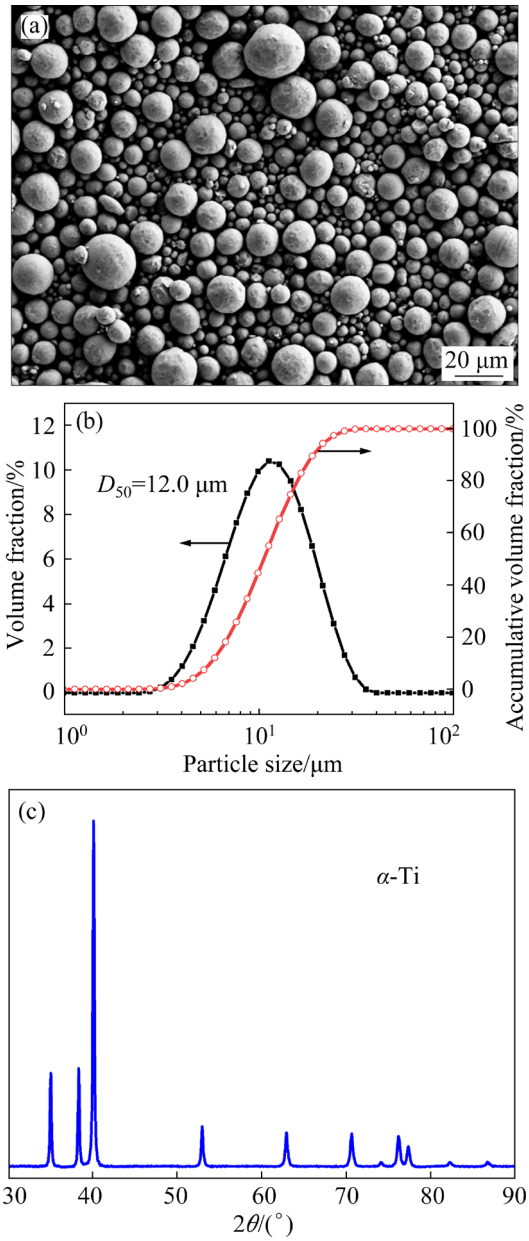

Fig. 4 Morphology (a), particle size distribution (b) and XRD pattern (c) of TA2 powder

3.2 Microstructural characteristics

Figure 5 shows the optical micrographs of the cross-sectional morphologies of As-CS and As-SR. The titanium/steel composite plate with pure titaniumization in the welding area can be divided into three areas. On the left side, there is the pure titaniumization area (TA), consisting of S-Ti coating and TA2 cladding. In the middle, there is the bonding area (BA) between the S-Ti coating and the Q235 base material. On the right side, there is the titanium/steel composite plate base material area (BM). The composite interfaces in the b and c regions in Fig. 5(a) were observed by high magnification optical microscope, and their morphologies are shown in Fig. 5(b) and Fig. 5(c), respectively. The composite interfaces between the S-Ti coating and titanium/steel composite plate exhibit a serrated pattern, without obvious holes and other defects, and the bonding quality is excellent. After hot rolling, the raised part of BA becomes flat (Fig. 5(d)), the S-Ti/TA2 interface disappears (Fig. 5(e)), and the S-Ti/Q235 interface still retains the serrated shape (Fig. 5(f)), which is conducive to enhancing the interfacial bonding strength. The composite interface in the TA belongs to the same metal combination of S-Ti coating and TA2 cladding, which can avoid the formation of harmful IMCs and achieve strong metallurgical bonding during subsequent hot rolling with large plastic strain [29]. Conversely, the BA represents the lateral bonding of dissimilar metals between the S-Ti coating and the Q235 matrix layer. In this area, the presence of Fe and Ti elements readily leads to the formation of the Fe−Ti phase under high temperature environment,

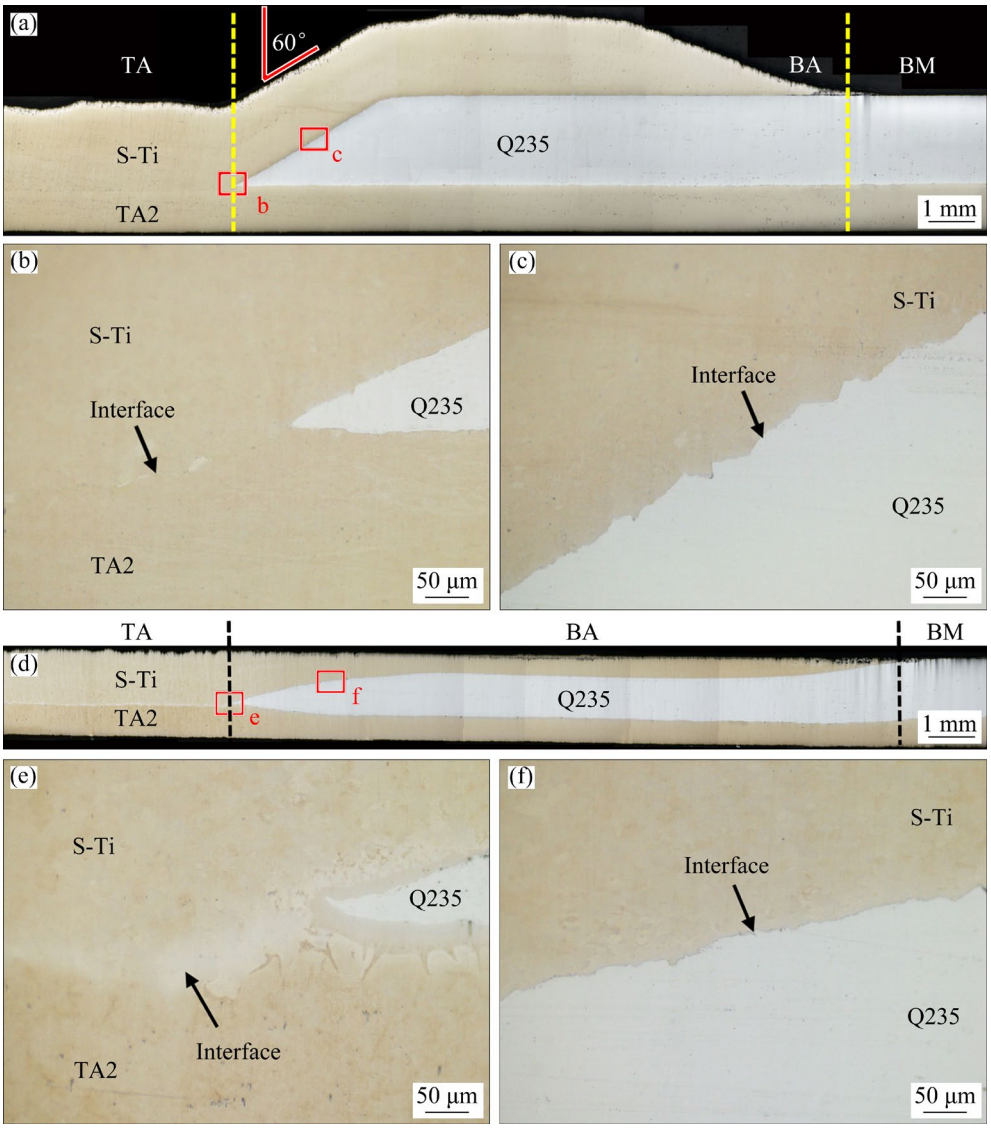

Fig. 5 Optical micrographs of cross-sectional morphologies of titanium/steel composite plate with pure titaniumization in welding area: (a−c) As-CS; (d−f) As-SR

which is unfavorable for interfacial composite. Therefore, achieving a high-quality composite of S-Ti and Q235 is crucial for preparing a high-strength titanium/steel composite plate with pure titanium-zation in the welding area. The following will mainly focus on the BA for in-depth study.

Figure 6 shows the XRD patterns of the S-Ti/Q235 peeling interfaces of As-CS, As-SH, As-SR and As-SRT samples. As shown in the figure, only the α-Ti and α-Fe phases are identified on the S-Ti/Q235 peeling composite interface of As-CS, indicating that the composite interface did not undergo alloying reaction. In addition, besides α-Ti and α-Fe phases, the TiC phase is identified on the S-Ti/Q235 peeling composite interfaces of As-SH, As-SR and As-SRT samples, but no other IMCs are detected. There are no Fe−Ti brittle phases at the S-Ti/Q235 composite interfaces of As-CS, As-SR and As-SRT samples under this preparation process.

Figure 7 shows the microstructure morphology and element distribution characteristics of As-CS, As-SH, As-SR and As-SRT samples. It can be clearly observed that the spherical TA2 powder particles have undergone large plastic deformation into ellipsoid shape by cold spraying deposition in Fig. 7(a1). A few holes exist between the TA2 particles, and the porosity of the coating is measured to be only 1.2%. After heating before hot rolling, the ellipsoidal TA2 particles have been recovered and recrystallized, forming multiple polygonal grains inside the particles with polygonal interfaces (Fig. 7(b1)), which is consistent with the research reported by LI et al [21]. After hot rolling deformation, the ellipsoidal TA2 particles are combined into a whole (Fig. 7(c1)), and then the microstructure morphology is not significantly changed by the high-temperature short-time heat treatment (Fig. 7(d1)). The microstructural evolution of the S-Ti/Q235 interface of As-CS, As-SH, As-SR and As-SRT samples was analyzed as follows. Obvious diffusion layers of Ti and Fe elements without C enrichment are detected at the S-Ti/Q235 composite interface in the As-CS (Fig. 7(a2)). The thickness of the Fe−Ti diffusion layer (DL) is about 1 μm by EDS line-scan analysis, and there are no oxides and carbides generated (Fig. 7(a3)). By heating before hot rolling, the DL thickness increases to 1.2 μm, and a significant C-element enrichment is observed (Fig. 7(b2)). EDS analysis indicates that the thickness of the formed TiC layer is about 0.7 μm (Fig. 7(b3)). The thicknesses of the C-element-enriched layer and the DL at the S-Ti/Q235 interface are slightly increased by the hot rolling process (Fig. 7(c2)), and their thicknesses are about 1.4 and 1.3 μm, respectively (Fig. 7(c3)). After heat treatment, the S-Ti/Q235 interface remains composed of TiC layer (1.4 μm) and DL (1.2 μm), and the heat treatment process does not alter the interfacial phase composition (Figs. 7(d2, d3)).

Figures 8 and 9 show the morphology and elemental distribution of the S-Ti/Q235 composite interface for As-SR and As-SRT, respectively. The S-Ti/Q235 composite interface is tightly bonded, exhibiting an overall serrated morphology, with the presence of nanoscale riveted structures locally, as shown in Fig. 8(a) and Fig. 9(a). The elemental distribution analysis of the S-Ti/Q235 interface of As-SR reveals no obvious diffusion of Fe and Ti elements, but there is a large amount of C enrichment on the Ti side, as shown in Fig. 8(b). High-resolution

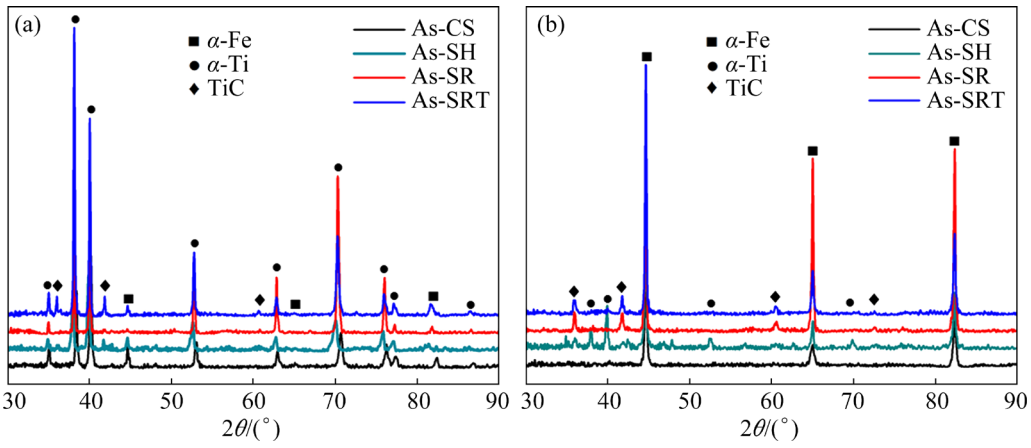

Fig. 6 XRD patterns of S-Ti/Q235 peeling interfaces of As-CS, As-SR and As-SRT samples: (a) On titanium side; (b) On steel side

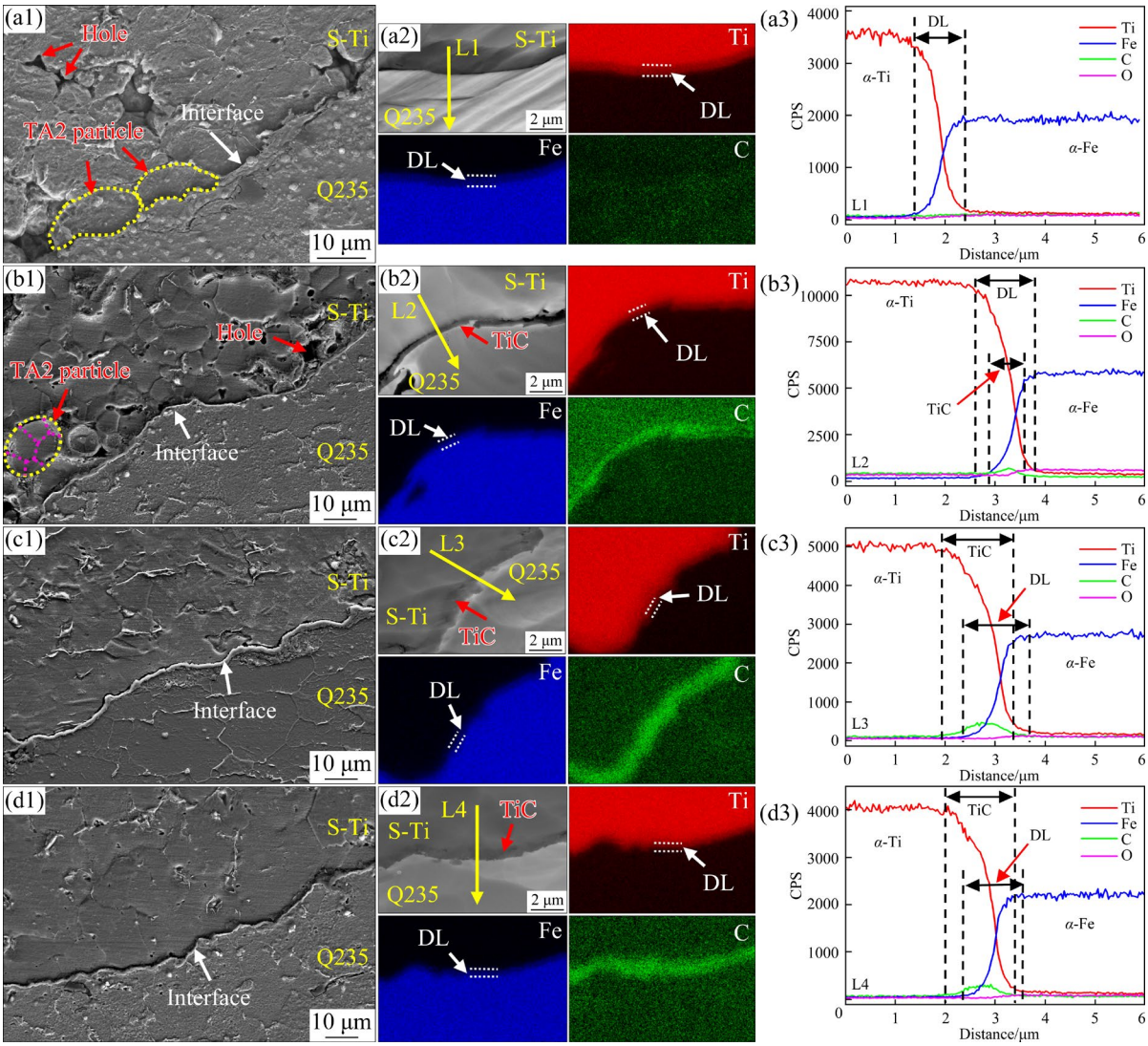

Fig. 7 Interface morphologies and elemental distributions of As-CS (a1−a3), As-SH (b1−b3), As-SR (c1−c3) and As-SRT (d1−d3) samples: (a1−d1) Low magnification images; (a2−d2) High magnification images and elemental distributions; (a3−d3) EDS line scan results of L1−L4 in (a2−d2), respectively

observation of the composite interface between the C-enriched region and the steel reveals the formation of TiC phase at the C-enriched site, while no obvious Fe−Ti phase exists, as shown in Fig. 8(c). EDS analysis indicates that the thickness of the TiC layer is about 1.3 μm, as shown in Fig. 8(d). After high-temperature short-time heat treatment, there is still no obvious diffusion of Fe and Ti elements at the S-Ti/Q235 interface of As-SRT. C element is enriched on the Ti side to form TiC phase with the thickness of about 1.0 μm, and the Fe−Ti phase is still not generated at the interface, as shown in Figs. 9(b−d).

Figure 10 presents the recrystallization distribution at the S-Ti/Q235 composite interface for As-SH, As-SR and As-SRT. As can be seen in Figs. 10(a, b), heating prior to hot rolling brings the As-SR sample to a high recrystallization state, with the percentage of recrystallization region exceeding 90% and that of deformed region falling below 2%. After the hot rolling process, the percentage of the deformed region in the S-Ti layer of the As-SR sample increases to 81.7%, while the recrystallization region makes up only 3.0%; Meanwhile, the percentage of the deformed region in the Q235 steel layer increases to 31.2%, and the recrystallization region accounts for only 1.7%, as shown in Figs. 10(c, d). Following heat treatment, the percentage of the deformed region in the S-Ti layer of As-SRT decreases to 10.6%, and the recrystallization region recovers to 63.6%; Similarly,

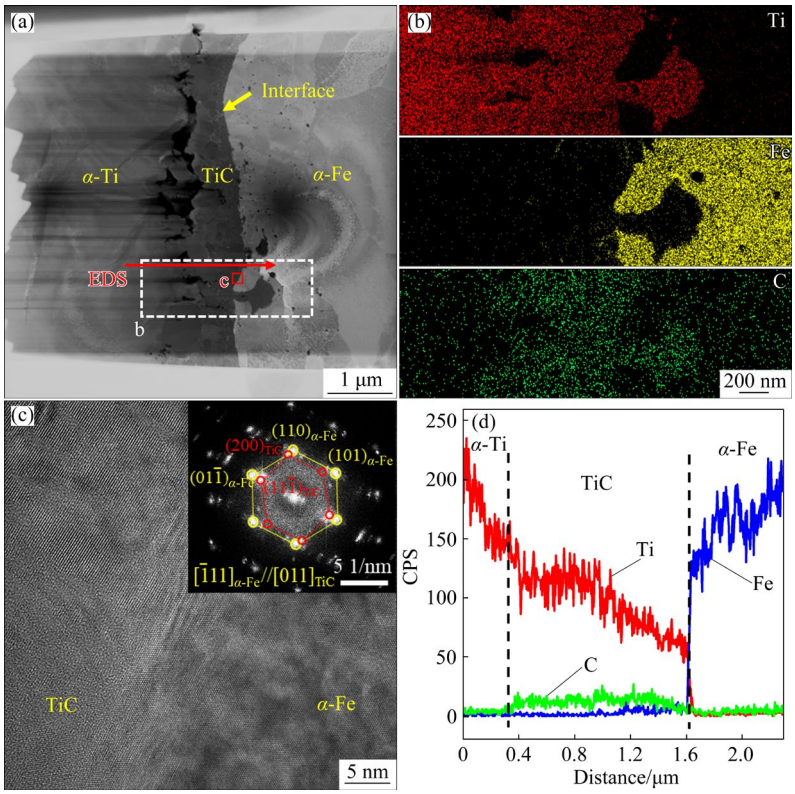

Fig. 8 Interface morphology (a−c) and elemental distribution (d) of S-Ti/Q235 composite interface for As-SR sample: (a) Interface morphology; (b) Element distribution in region b of (a); (c) High-resolution image of composite interface in region c of (a); (d) EDS line scan results in (a)

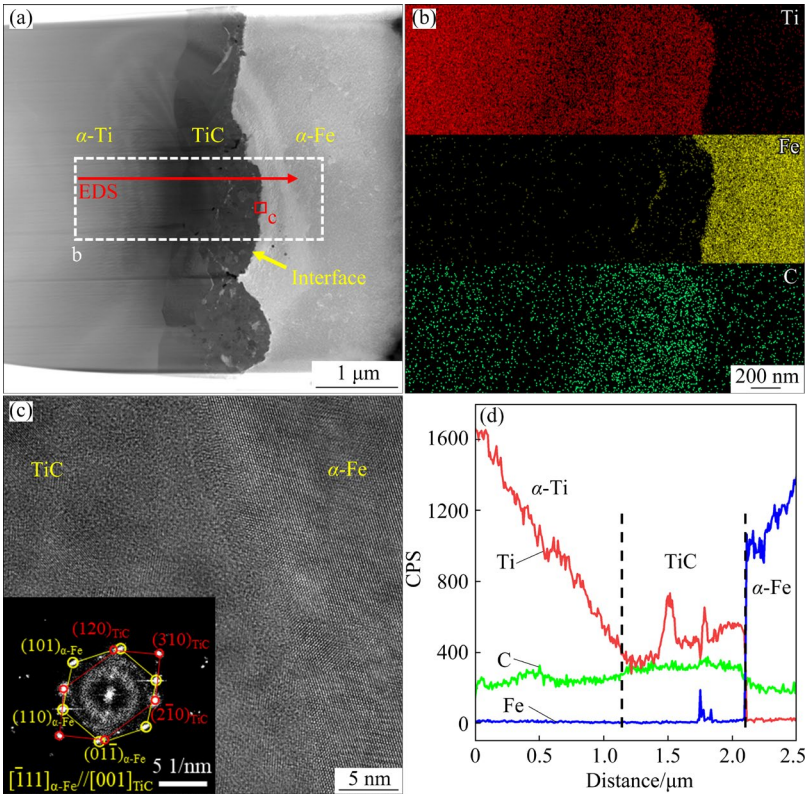

Fig. 9 Interface morphology (a−c) and elemental distribution (d) of S-Ti/Q235 composite interface for As-SRT sample: (a) Interface morphology; (b) Element distribution in region b of (a); (c) High-resolution image of composite interface in region c in (a); (d) EDS line scan results in (a)

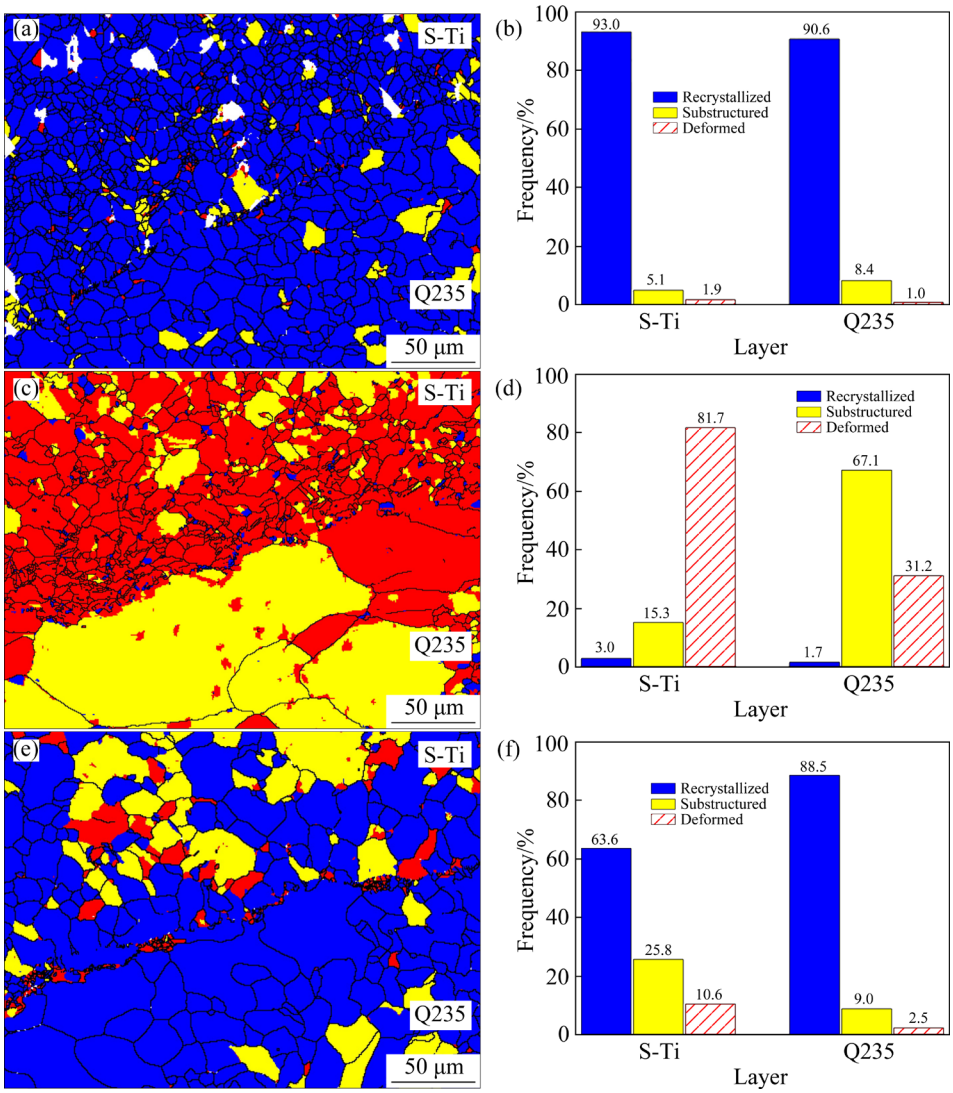

Fig. 10 Recrystallization distribution of S-Ti/Q235 composite interface for As-SH (a, b), As-SR (c, d) and As-SRT (e, f) samples

the percentage of the deformed region in the Q235 steel layer decreases to only 2.5%, and the recrystallization region recovers to 88.5%, as shown in Figs. 10(e, f). After heat treatment, the welding area with pure titaniumization of the titanium/steel composite plate exhibits a higher recrystallization recovery state, effectively reducing the stress concentration within the grains.

3.3 Mechanical properties and fracture morphology

Figures 11(a, b) show the tensile mechanical properties of As-SR and As-SRT. The yield strength (YS) of As-SR is 310 MPa, the tensile strength (UTS) is 346 MPa, and the elongation at fracture (EL) is only 0.3%. After heat treatment, the YS of As-SRT is 289 MPa, the UTS reaches 414 MPa, and the EL reaches 7.2%. The UTS of As-SRT reaches 95.6% of the UTS (433 MPa) of titanium/steel composite plate (As-SRT$_{(T/Q)}$) after the same process. Figures 11(c, d) show the shear test results of As-SR and As-SRT. After hot rolling, the interfacial bonding strength of As-SR is 276 MPa, while there is a smaller decrease to 257 MPa after heat treatment. The interfacial bonding strength of the sample is higher than that of the titanium/steel composite plates fabricated by conventional hot-rolling process [30,31]. In short, the titanium/steel composite plate with pure titaniumization in the welding area exhibits excellent mechanical properties.

Figure 12 presents the tensile fracture morphologies of As-SR and As-SRT samples. The fracture primarily occurred near the junction region

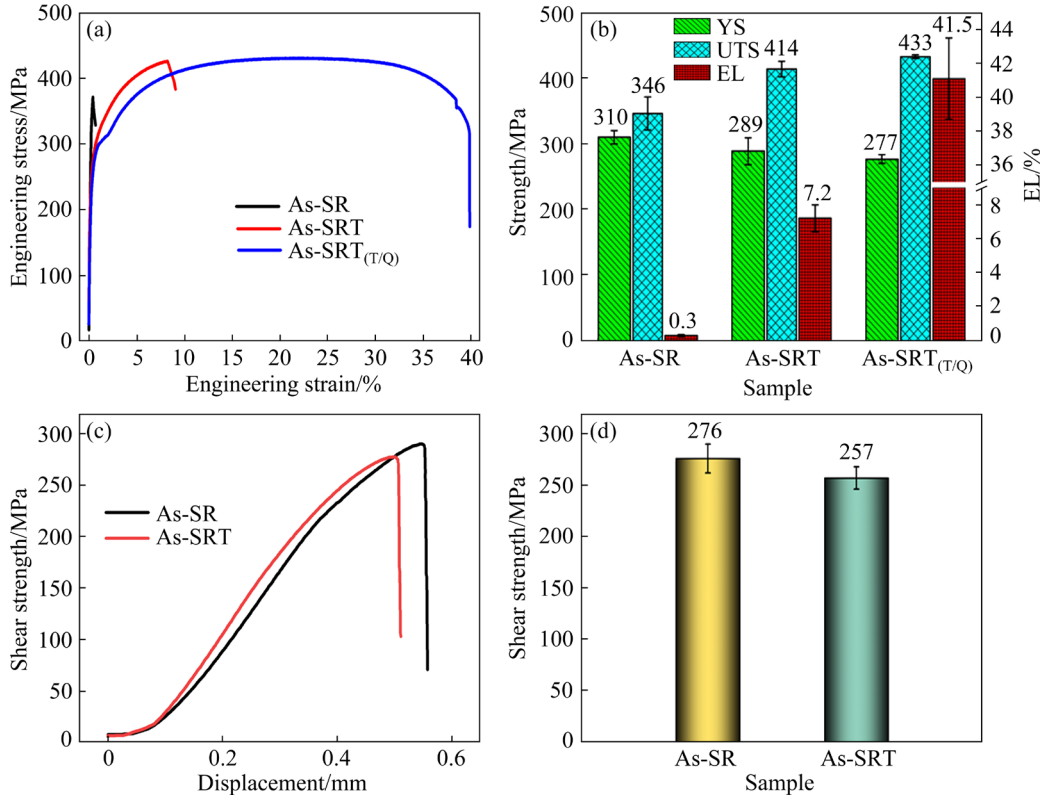

Fig. 11 Mechanical properties of As-SR and As-SRT samples: (a, b) Tensile test results; (c, d) Shear test results

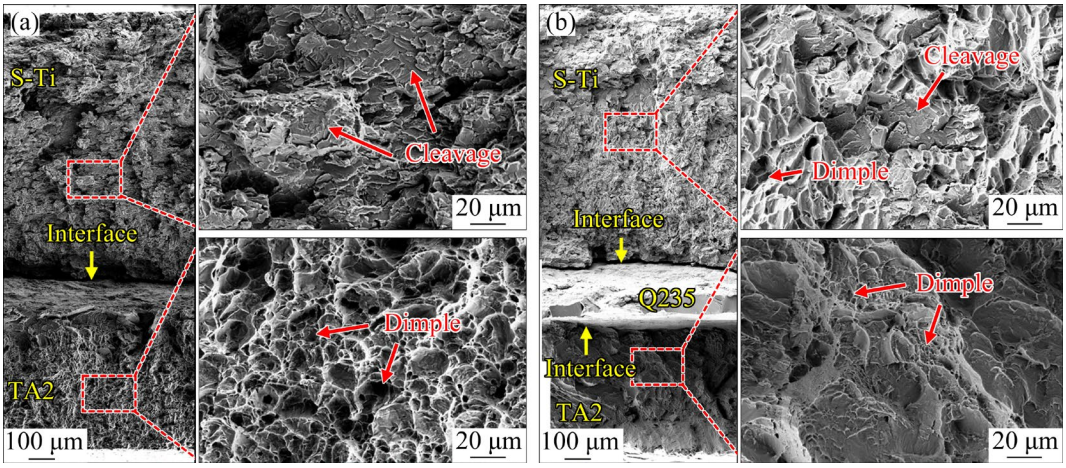

Fig. 12 Morphologies of samples after tensile fracture: (a) As-SR; (b) As-SRT

of TA and BA. For the As-SR sample, the fracture of TA2 cladding is dominated by dimples, and the fracture of S-Ti coating is dominated by cleavage platforms, as shown in Fig. 12(a). In the As-SRT sample, the fracture of TA2 cladding is still dominated by dimples, and the fracture of S-Ti coating is a mixture of cleavage platform and dimples, as shown in Fig. 12(b). After heat treatment, the S-Ti coating transforms from a brittle fracture to a ductile-brittle hybrid fracture, resulting in an improvement in its plasticity.

4 Discussion

The pure titaniumization in the welding area of titanium/steel composite plate can be mainly divided into several steps: the structure processing of the trapezoidal composite interface, cold spraying deposition composite, heating, hot rolling and heat treatment. The composite interface to be deposited by cold spraying is designed as a trapezoidal structure. Compared to directly cold spraying a

thicker pure titanium layer onto the end face of the titanium/steel composite plate, the trapezoidal structure is transformed from the end face to the flat surface, making it easier to achieve dimensional control of the pure titaniumization area. This not only reduces the difficulty of composite but also increases the bonding area of the composite interface. In addition, it also solves the challenge of cold spraying deposition composite of the end face of the thin thickness of MLCP.

In the process of cold spraying deposition, the high speed TA2 powder impacts the surface of the substrate, causing the spherical particles to deform into ellipsoidal shapes due to adiabatic shear plastic deformation. This deformation results in the composite interface being in a state of mechanical locking and local metallurgical bonding [20]. The Fe−Ti element diffusion layer is formed at the S-Ti/Q235 composite interface, but the short particle impact time prevents phase transition and the generation of IMCs (Figs. 7(a2, a3)). In addition, the composite interface is not significantly oxidized under the lower process temperature and the protection of nitrogen atmosphere (Fig. 7(a3)). Generally, achieving a fully bonded interface by cold spraying deposition is difficult [32]. The mechanical properties of the cold-sprayed S-Ti coating are poor due to the presence of unbonded holes at the local interface. The deposition of TA2 powder by cold spraying realizes the pure titaniumization in the welding area of titanium/steel composite plate. Meanwhile, the pre-deposited interface can prevent interface contamination from oxygen in the high-temperature environment, allowing for direct processing without atmosphere protection for hot rolling plasticity strengthening [33].

In the rolling composite process, the higher temperature is more conducive to the diffusion of elements between the metals, thus improving the interfacial bond strength. However, during the hot rolling composite process of titanium and steel, the generated β-Ti is easy to promote the formation of Fe−Ti phase when the temperature is higher than the phase transition temperature (882 °C) of β-Ti [33]. Particularly when the hot rolling temperature exceeds 950 °C, a micrometer-thick Fe−Ti IMC layer can be formed at the titanium/steel composite interface, which decreases the properties of the interface [20,26]. Titanium/steel composite plates are hot rolled at a higher temperature of 850 °C, which can avoid the formation of Fe−Ti phases at the composite interface [33]. In addition, the order of the standard molar generation Gibbs free energy change from high to low at the same temperature is FeTi > Fe_2Ti > TiC, thus TiC is most easily generated at the composite interface [34]. As the diffusion rate of the C atom in TiC is four orders of magnitude higher than that of Fe atom [35], the TiC can hinder the diffusion of Fe and Ti atoms and avoid Fe−Ti phase generation [33,36].

Therefore, in this study, a heating temperature lower than the phase transition temperature of β-Ti before hot rolling is adopted, along with sufficient insulation time to pre-generate a continuous TiC layer at the interface (Figs. 7(b2, b3)), thus hindering the alloying reaction between Fe and Ti during the hot rolling process. As a result, there is still TiC at the S-Ti/Q235 interface after hot rolling, and no Fe−Ti phase is generated (Fig. 6 and Fig. 7). Hot rolling eliminates the internal defects in the coating and enhances the properties of metallurgical bonding between the particles. However, it also produces work hardening, leading to the formation of numerous dislocations within the metal, causing lattice distortion to generate internal stresses, which reduce the plasticity of the metal [20]. It can be seen from Fig. 10 that hot rolling results in the internal grains of the metal being in a higher state of deformation with higher stress concentrations. Heat treatment can promote the grain recovery and recrystallization, significantly reducing the number of dislocations within the metal and thereby improving its plasticity [37]. When the heat treatment temperature exceeds the phase transition temperature of β-Ti, the TiC at the interface will gradually decompose, preventing further thickening of the TiC layer. However, prolonged heat treatment can lead to the formation of Ti−Fe phases at the interface, which will affect the interface bonding properties. Adopting a temperature slightly above the phase transition temperature of β-Ti for short-time heat treatment can prevent excessive thickening of the TiC layer at the interface. Simultaneously, it significantly reduces the high dislocation density within the metal, thus improving the comprehensive performance of the welding area with pure titaniumization of the titanium/steel composite plate.

Dislocations can be classified as geometrically

necessary dislocation (GND) and statistical storage dislocation (SSD). Among them, GND causes lattice distortion while SSD does not, so the degree of lattice distortion within the crystal structure can be reflected by GND. The average geometrically necessary dislocation density ($\rho_{avg.}^{GND}$) within the metal can be calculated by kernel average misorientation (KAM) [38]. According to the strain gradient theory [39], Eq. (1) is used to calculate the $\rho_{avg.}^{GND}$:

$$\rho_{avg.}^{GND}=\frac{2KAM_{avg.}}{\mu b} \tag{1}$$

where $KAM_{avg.}$ is the average value of KAM, μ is the scanning step of EBSD (μ=0.6 μm), and b is the magnitude of Burgers vector (with the b of TA2 taken as 0.289 nm [40], and that b of Q235 taken as 0.248 nm [41]).

The KAM distribution in the S-Ti/Q235 composite interfacial regions of As-SH, As-SR and As-SRT is analyzed, and the results are shown in Fig. 13. The $KAM_{avg.}$ values of S-Ti coating and Q235 steel in As-SH sample are 0.35° and 0.21°, respectively. The $\rho_{avg.}^{GND}$ values of S-Ti coating and Q235 steel are calculated from the $KAM_{avg.}$ to be 0.70×10^{14} and 0.49×10^{14} m^{-2}, respectively, as shown in Figs. 13(a−c). After hot rolling, the $KAM_{avg.}$ is 1.52° for the S-Ti coating and 0.96° for the Q235 steel of the As-SR samples, and the $\rho_{avg.}^{GND}$ values of the S-Ti coating and the Q235 steel are significantly increased to 3.06×10^{14} and 2.25×10^{14} m^{-2}, respectively, as shown in Figs. 13(d−f). After heat treatment, the $KAM_{avg.}$ values are 0.50° for the S-Ti coating and 0.21° for the Q235 steel of As-SRT samples, and the $\rho_{avg.}^{GND}$ values of the S-Ti coating and the Q235 steel are reduced to 1.01×10^{14} and 0.49×10^{14} m^{-2}, respectively, as shown in Figs. 13(g−i).

Through the hot rolling process, high-density dislocations and large internal stresses are generated within the As-SR samples (Fig. 13). In particular, the percentage of deformation structure in the S-Ti coating is as high as 81.7% (Fig. 10(d)). The metal

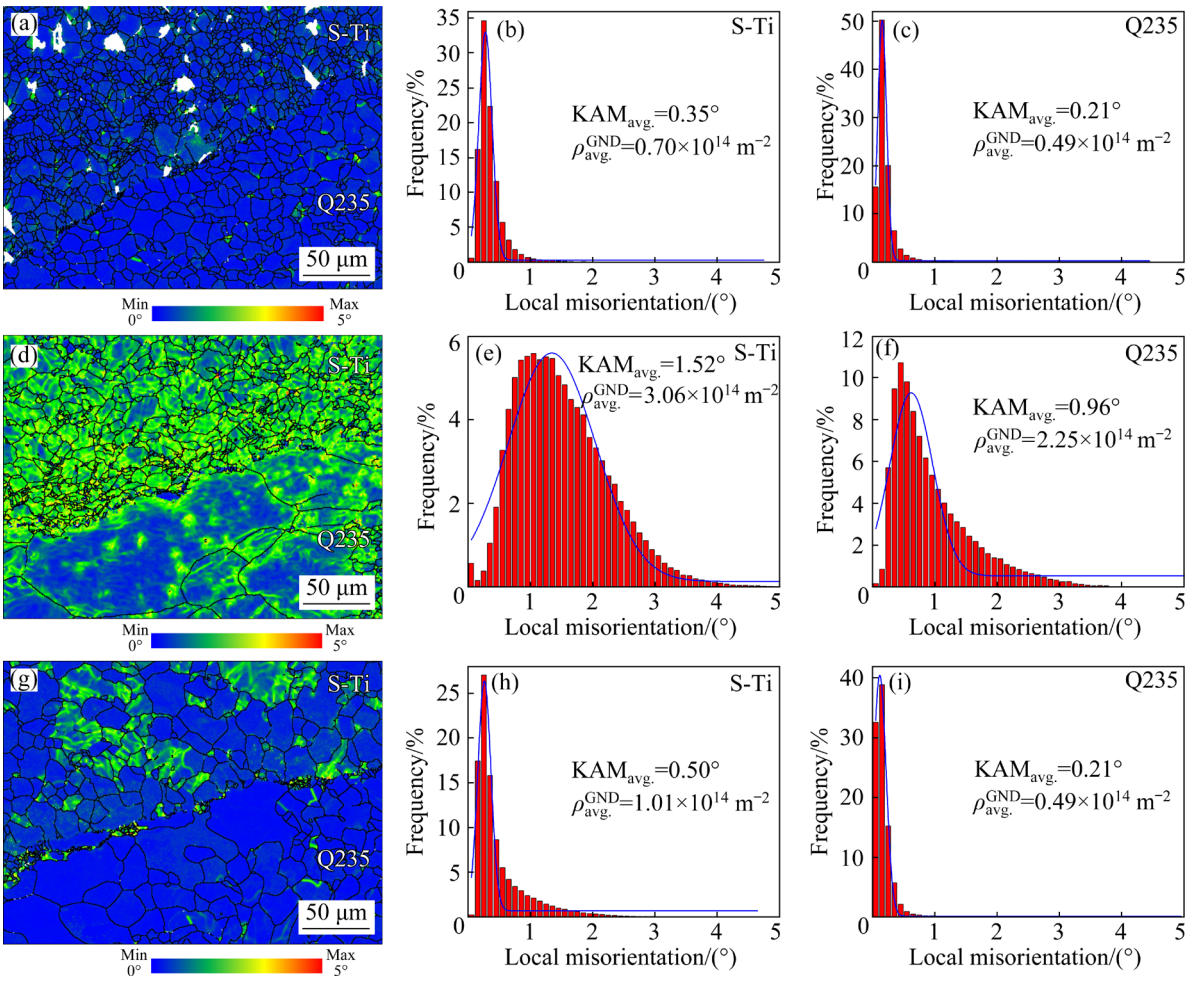

Fig. 13 KAM distribution of S-Ti/Q235 composite interfaces: (a−c) As-SH; (d−f) As-SR; (g−i) As-SRT

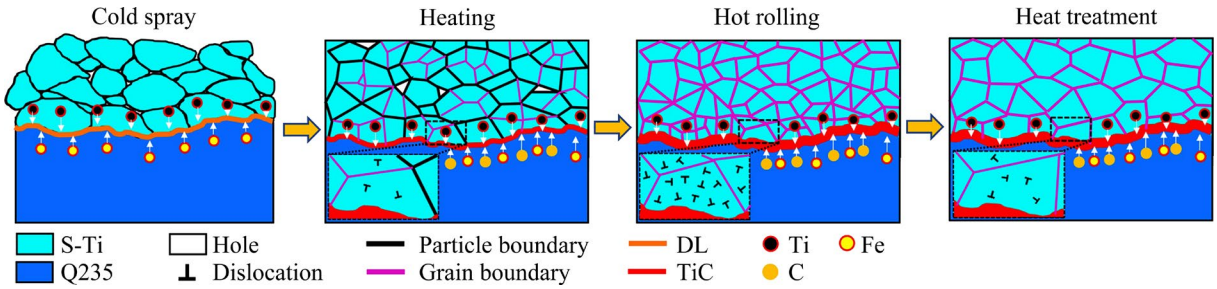

Fig. 14 Schematic diagram showing microstructural evolution of S-Ti/Q235 composite interface during pure titaniumization in welding area of titanium/steel composite plate

work hardening is severe, leading to brittle fracture in the pure titaniumization area (Fig. 12). The tensile strength of As-SR sample is less than 80% of that of the base material, and the elongation at fracture is only 0.3% (Fig. 11). The As-SR sample undergoes heat treatment with high-temperature short-time, which does not change the physical phase composition of the interface (Fig. 6 and Fig. 7), but significantly reduces the density of dislocations and internal stresses within the coating (Figs. 13(g−i)). The percentage of recrystallized structure within the S-Ti coating reaches 63.6% (Fig. 10(f)). The heat treatment improves the overall plastic deformability of the welding area with pure titaniumization of the titanium/steel composite plate. The tensile strength of As-SRT sample reaches 95.6% of that of the base material, and the elongation at fracture increases by about 24 times compared to that of the As-SR sample (Fig. 11).

Figure 14 shows the microstructure evolution of the S-Ti/Q235 composite interface during the pure titaniumization in the welding area of the titanium/steel composite plate. As can be seen from the figure, the initially spherical TA2 particles undergo ellipsoidal transformation due to high-speed impact adiabatic shear plastic deformation. The composite interface is formed through a combination of mechanical locking and local metallurgy, resulting in the formation of a Fe−Ti diffusion layer at the S-Ti/Q235 composite interface. During the heating process preceding rolling, the TA2 particles undergo recovery and recrystallization, resulting in the formation of multiple equiaxed crystal grains within them. A strong metallurgical bond is established between the particles, and their boundaries transform into polygonal shapes. In addition, C atoms from the Q235 steel side diffuse into the S-Ti/Q235 composite interface, facilitating the formation of a continuous TiC layer. Following the hot rolling process, the TiC layer thickens, while the S-Ti/Q235 composite interface retains its structure with the TiC layer, without generating any Fe−Ti phases. The TA2 powder particles undergo consolidation under large deformation; however, a high density of dislocations forms within the metal, resulting in reduced ductility. After heat treatment, the grains in the S-Ti coating recover and recrystallize, the dislocation density decreases significantly, and the plasticity and strength increase greatly.

5 Conclusions

(1) The high-strength titanium/steel composite plate with pure titaniumization in the welding area is prepared by cold spraying, hot rolling and heat treatment processes. The tensile strength is 414 MPa, which is 95.6% of the tensile strength of the base material of titanium/steel composite plate.

(2) The TA2 powder is deposited in the welding area of the titanium/steel composite plate by cold spraying technology, and the S-Ti/Q235 composite interface does not generate any intermetallic compounds. The continuous TiC layer generated through heating hinders the alloying reaction of the Fe and Ti elements during the hot rolling or heat treatment process. The interfacial binding strength is up to 257 MPa.

(3) Hot rolling promotes strong metallurgical bonding between titanium particles and eliminates internal defects in coatings. Heat treatment can promote recrystallization and reduce the dislocation density of the coating without changing the phase composition of the composite interface, which significantly improves the plasticity of the titanium/steel composite plate with pure titaniumization in the

welding area. As a result, the elongation at fracture increases by 24 times compared to that of the hot-rolled state.

CRediT authorship contribution statement

Hong-ting CHEN: Conceptualization, Methodology, Experiment, Investigation, Writing − Original draft, Writing − Review & editing; **Xue-feng LIU:** Conceptualization, Supervision, Validation, Writing − Review & editing, Funding acquisition; **Zhi-yan YANG:** Experiment, Investigation; **Xiao-liang LU:** Experiment, Investigation.

Declaration of competing interest

The authors declare that they have no known competing financial interests or personal relationships that could have appeared to influence the work reported in this paper.

Acknowledgments

This work was financially supported by the National Key R&D Program of China (No. 2018YFA0707300), and the National Natural Science Foundation of China (No. 52374376).

References

[1] BAI Yu-liang, LIU Xue-feng, WANG Wen-jing, YANG Yao-hua. Current status and research trends in processing and application of titanium/steel composite plate [J]. Chinese Journal of Engineering, 2021, 43(1): 85−96. (in Chinese)

[2] LIU Jiang-jiang, CHEN Ze-jun, ZHOU Zhan-song, MO Tai-qian, WANG Peng-ju, HE Wei-jun. Microstructure evolution, mechanical properties and tailoring of coefficient of thermal expansion for Cu/Mo/Cu clad sheets fabricated by hot rolling [J]. Transactions of Nonferrous Metals Society of China, 2022, 32(7): 2290−2308.

[3] ZHU Min, WU Wei, QIAN Wei-fang, XIA Li-qian, ZHANG Yan-song, WANG Bao-sen. A brief review on welding of stainless steel clad plates: Issues and future perspectives [J]. The International Journal of Advanced Manufacturing Technology, 2021, 115(1/2): 49−59.

[4] CHU Qiao-ling, TONG Xiong-wei, XU Shu-ai, ZHANG Min, YAN Fu-xue, CHENG Peng, YAN Cheng. The formation of intermetallics in Ti/steel dissimilar joints welded by Cu−Nb composite filler [J]. Journal of Alloys and Compounds, 2020, 828: 154389.

[5] NING Jie, ZHANG Lin-jie, JIANG Gui-chuan, XIE Miao-xia, YIN Xian-qing, ZHANG Jian-xun. Narrow gap multi-pass laser butt welding of explosion welded CP-Ti/Q235B bimetallic sheet by using a copper interlayer [J]. Journal of Alloys and Compounds, 2017, 701: 587−602.

[6] WANG Ting, WANG Hao, LI Ning, JIANG Si-yuan, CHU Qiao-ling, WANG Wen-hui. Microstructural and mechanical heterogeneity of electron beam welded thick pure titanium/Q235B steel bimetallic plate joint [J]. Journal of Materials Engineering and Performance, 2023, 32(12): 5273−5282.

[7] ZHANG Hai-bo, ZHANG Lin-jie, LIU Jiang-zhe, NING jie, ZHANG Jian-xun, NA S J, ZHU Lei. Microstructures and performances of the butt joint of TA1/Q235B bimetallic sheet with addition of a Mo interlayer by using narrow gap laser welding with filler wire [J]. Journal of Materials Research and Technology, 2020, 9(5): 10498−10510.

[8] DING Yun-long, WANG Jian-gang, ZHAO Ming, JU Dong-ying. Effect of annealing temperature on joints of diffusion bonded Mg/Al alloys [J]. Transactions of Nonferrous Metals Society of China, 2018, 28(2): 251−258.

[9] LU Wen-bin, ZHANG Yan, GUO Zhi-jin, LIU Yu-qiang, YU De-shui. Double laser welding of TC4 alloy and 304 stainless steel using an explosion welded composite plate as an interlayer [J]. Materials Letters, 2023, 330: 133382.

[10] TRICARICO L, SPINA R. Experimental investigation of laser beam welding of explosion-welded steel/aluminum structural transition joints [J]. Materials & Design, 2010, 31(4): 1981−1992.

[11] ZHANG Yan, GAO Yi-di, ZHOU Jian-ping, SUN Da-qian, LI Hong-mei. Microstructure and mechanical property improvement of dissimilar metal joints for TC4 Ti alloy to 304 stainless steel using TA2/Q235 composite interlayer [J]. Metals and Materials International, 2021, 27(5): 1224−1235.

[12] ZHANG Yan, GAO Yi-di, YU De-shui, ZHOU Jian-ping, SUN Da-qian. Preparation of high-strength TC4/304 dissimilar joint with TA2/304 composite interlayer by a dual-pass laser [J]. Optics & Laser Technology, 2022, 154: 108298.

[13] CHENG Xian-ming, YANG Ke, LIU Si-zhan, JI Shan-lin, WANG Jian. Microstructure and mechanical properties of ultrasonic welded copper to aluminum cables joints [J]. Transactions of Nonferrous Metals Society of China, 2023, 33(10): 3027−3038.

[14] LI Ning, ZHANG Min, YE Jian-lin, LIU Chuan. Experimental investigation on residual stress distribution in zirconium/titanium/steel tri-metal explosively welded composite plate after cutting and welding of a cover plate [J]. Journal of Manufacturing Processes, 2021, 64: 455−463.

[15] LI Wen-ya, CAO Cong-cong, YIN Shuo. Solid-state cold spraying of Ti and its alloys: A literature review [J]. Progress in Materials Science, 2020, 110: 100633.

[16] YIN Shuo, CAVALIERE P, ALDWELL B, JENKINS R, LIAO Han-lin, LI Wen-ya, LUPOI R. Cold spray additive manufacturing and repair: Fundamentals and applications [J]. Additive Manufacturing, 2018, 21: 628−650.

[17] REN Yu-peng, TARIQ N U H, LIU Han-hui, CUI Xin-yu, SHEN Yan-fang, WANG Ji-qiang, XIONG Tian-ying. An innovative and flexible approach to fabricate Mg/Al composite plates: Cold spraying and hot rolling post-treatment [J]. Materials Science and Engineering A, 2022, 849: 143515.

[18] SENG D H L, ZHANG Z, ZHANG Z Q, MENG T L, TEO S L, TAN B H, LOI Q, PAN J S, BA T. Impact of spray angle

and particle velocity in cold sprayed IN718 coatings [J]. Surface and Coatings Technology, 2023, 466: 129623.

[19] YIN Shuo, FAN Ning-song, HUANG Chun-jie, XIE Ying-chun, ZHANG Chao, LUPOI R, LI Wen-ya. Towards high-strength cold spray additive manufactured metals: Methods, mechanisms, and properties [J]. Journal of Materials Science & Technology, 2024, 170: 47−64.

[20] ZHAO Zhi-po, TARIQ N U H, TANG Jun-rong, JIA Cun-lei, QIU Xiang, REN Yu-peng, LIU Han-hui, SHEN Yan-fang, DU Hao, CUI Xin-yu, WANG Ji-qiang, XIONG Tian-ying. Microstructural evolutions and mechanical characteristics of Ti/steel clad plates fabricated through cold spray additive manufacturing followed by hot-rolling and annealing [J]. Materials & Design, 2020, 185: 108249.

[21] LI Zhi-ming, YANG Xiao-ping, ZHANG Jun-bao, ZHENG Bao-long, ZHOU Yi-zhang, SHAN Ai-dang, LAVERNIA E J. Microstructure evolution and mechanical behavior of cold-sprayed, bulk nanostructured titanium [J]. Metallurgical and Materials Transactions A, 2014, 45(11): 5017−5028.

[22] NIKBAKHT R, SEYEDEIN S H, KHEIRANDISH S, ASSADI H, JODOIN B. Asymmetrical bonding in cold spraying of dissimilar materials [J]. Applied Surface Science, 2018, 444: 621−632.

[23] XIONG Yu-ming, ZHUANG W, ZHANG Ming-xing. Effect of the thickness of cold sprayed aluminium alloy coating on the adhesive bond strength with an aluminium alloy substrate [J]. Surface and Coatings Technology, 2015, 270: 259−265.

[24] REN Y Q, KING P C, YANG Y S, XIAO T Q, CHU C, GULIZIA S, MURPHY A B. Characterization of heat treatment-induced pore structure changes in cold-sprayed titanium [J]. Materials Characterization, 2017, 132: 69−75.

[25] ZAHIRI S H, ANTONIO C I, JAHEDI M. Elimination of porosity in directly fabricated titanium via cold gas dynamic spraying [J]. Journal of Materials Processing Technology, 2009, 209(2): 922−929.

[26] ZHAO Zhi-po, TANG Jun-rong, TARIQ N U H, LIU Hou-sheng, LIU Han-hui, REN Yu-peng, TONG Min, YIN Li-song, DU Hao, WANG Ji-qiang, XIONG Tian-ying. Effect of rolling temperature on microstructure and mechanical properties of Ti/steel clad plates fabricated by cold spraying and hot-rolling [J]. Materials Science and Engineering A, 2020, 795: 139982.

[27] LI Zhi-ming, YANG Xiao-ping, ZHANG Jun-bao, SHAN Ai-dang. Interfacial mechanical behavior and electrochemical corrosion characteristics of cold-sprayed and hot-rolled titanium/stainless-steel couples [J]. Advanced Engineering Materials, 2016, 18(7): 1240−1249.

[28] BAI Yu-liang, LIU Xue-feng, SHI Zhang-zhi. Stress-induced alternating microstructures of titanium/steel bonding interface [J]. Materials Letters, 2021, 298: 130019.

[29] LIU W F, YUAN J J, LI S, GAO X W, WANG L, YAO J H, FAN Q B. Ti386/TC4 clad plate manufactured by hot rolling and solution-aging treatment [J]. Materials Letters, 2024, 354: 135390.

[30] LI B X, CHEN Z J, HE W J, WANG P J, LIN J S, WANG Y, PENG L, LI J, LIU Q. Effect of interlayer material and rolling temperature on microstructures and mechanical properties of titanium/steel clad plates [J]. Materials Science and Engineering A, 2019, 749: 241−248.

[31] CHAI Xi-yang, PAN Tao, CHAI Feng, LUO Xiao-bing, SU Hang, YANG Zhi-gang, YANG Cai-fu. Interlayer engineering for titanium clad steel by hot roll bonding [J]. Journal of Iron and Steel Research International, 2018, 25(7): 739−745.

[32] KING P C, BUSCH C, KITTEL-SHERRI T, JAHEDI M GULIZIA S. Interface melding in cold spray titanium particle impact [J]. Surface and Coatings Technology, 2014, 239: 191−199.

[33] BAI Yu-liang, LIU Xue-feng. Interfacial reaction behavior of titanium/steel composite plate formed by cold-hot rolling [J]. Materials Characterization, 2023, 202: 113030.

[34] LEI Xiao-ling, DING Wen-hong, HU Ying, WU Meng-xian, HOU Hua-dong. Structural modification of TA2/Q355B composite interface and study of TiC stability mechanism [J]. Materials Science and Technology, 2023, 39(15): 1939−1949.

[35] MIRIYEV A, SINDER M, FRAGE N. Thermal stability and growth kinetics of the interfacial TiC layer in the Ti alloy/carbon steel system [J]. Acta Materialia, 2014, 75: 348−355.

[36] YU Chao, FU Lun, XIAO Hong, LV Qiang, GAO Bo-xing. Effect of carbon content on the microstructure and bonding properties of hot-rolling pure titanium clad carbon steel plates [J]. Materials Science and Engineering A, 2021, 820: 141572.

[37] QIU Xiang, TARIQ N U H, QI Lu, ZAN Yu-ning, WANG Yu-jiang, WANG Ji-qiang, DU Hao, XIONG Tian-ying. In-situ Sip/A380 alloy nano/micro composite formation through cold spray additive manufacturing and subsequent hot rolling treatment: Microstructure and mechanical properties [J]. Journal of Alloys and Compounds, 2019, 780: 597−606.

[38] CALCAGNOTTO M, PONGE D, DEMIR E, RAABE D. Orientation gradients and geometrically necessary dislocations in ultrafine grained dual-phase steels studied by 2D and 3D EBSD [J]. Materials Science and Engineering A, 2010, 527(10/11): 2738−2746.

[39] KUBIN L P, MORTENSEN A. Geometrically necessary dislocations and strain-gradient plasticity: A few critical issues [J]. Scripta Materialia, 2003, 48(2): 119−125.

[40] CHEN Wen-huan, HE Wei-jun, LUO Nian-chun, TANG Yi-zhi, CHEN Ze-jun, JIANG Bin. Effect of layer thickness on the enhanced strength and ductility of laminated Ti/Al composite [J]. Materials Science and Engineering A, 2022, 859: 144230.

[41] SUN Yan-lan, LIU Xue-feng, WANG Wen-jing, YANG Yao-hua, ZHANG Wei-liang. Diffusion mechanism of immiscible Fe−Mg system induced by high-density defects at the steel/Mg composite interface [J]. Journal of Materials Science & Technology, 2023, 144: 150−160.

钛/钢复合板待焊区域在纯钛化制备过程中的显微组织演变与力学性能

陈虹廷[1,2,3]，刘雪峰[1,2,3]，杨智研[1,2,3]，卢晓亮[1]

1. 北京科技大学 北京材料基因工程高精尖创新中心，北京 100083；
2. 北京科技大学 现代交通金属材料与加工技术北京实验室，北京 100083；
3. 北京科技大学 材料先进制备技术教育部重点实验室，北京 100083

摘　要：将待焊区域的异种金属转化为单一金属是实现异种金属层状复合板高质量焊接连接的重要方法。本文采用冷喷涂、热轧和热处理工艺制备了高性能的待焊区域纯钛化的钛/钢复合板(TSCP)。结果表明，冷喷涂使钛颗粒实现了较好的沉积预复合，抑制了界面氧化和 Fe−Ti 合金化反应并形成了孔隙率仅为 1.2%的较致密的纯钛化涂层。热轧消除了涂层内部缺陷并促进了复合界面的强冶金结合。热处理促进了涂层再结晶，降低了涂层内部的位错密度。TSCP 的纯钛化待焊区域的界面结合强度为 257 MPa，抗拉强度为 414 MPa，为 TSCP 基材的 95.6%。

关键词：钛/钢复合板；冷喷涂；焊接过渡接头；显微组织；力学性能

(Edited by Wei-ping CHEN)